ASSESSMENT OF MODAL PUSHOVER-BASED SCALING PROCEDURE FOR NONLINEAR RESPONSE HISTORY ANALYSIS OF "ORDINARY STANDARD" BRIDGES

By Erol Kalkan[1] and Neal S. Kwong[2]

[1] U.S. Geological Survey, Menlo Park, CA 94025, *ekalkan@usgs.gov* (corresponding author)

[2] University of California, Berkeley, CA 94709, *nealsimonkwong@berkeley.edu*

ABSTRACT

The earthquake engineering profession is increasingly utilizing nonlinear response history analyses (RHA) to evaluate seismic performance of existing structures and proposed designs of new structures. One of the main ingredients of nonlinear RHA is a set of ground motion records representing the expected hazard environment for the structure. When recorded motions do not exist (as is the case for central U.S.) or when high-intensity records are needed (as is the case for San Francisco and Los Angeles), ground motions from other tectonically similar regions need to be selected and scaled. The modal-pushover-based scaling (MPS) procedure was recently developed to determine scale factors for a small number of records such that the scaled records provide accurate and efficient estimates of "true" median structural responses. The adjective "accurate" refers to the discrepancy between the benchmark responses and those computed from the MPS procedure. The adjective "efficient" refers to the record-to-record variability of responses. Herein, the accuracy and efficiency of the MPS procedure are evaluated by applying it to four types of existing "Ordinary Standard" bridges typical of reinforced concrete bridge construction in California. These bridges are the single-bent overpass, multi-span bridge, curved bridge and skew bridge. As compared to benchmark analyses of unscaled records using a larger catalog of ground motions, it is demonstrated that the MPS procedure provided accurate estimate of the EDPs accompanied by significantly reduced record-to-record variability of the EDPs. Thus it is a useful tool for scaling ground motions as input to nonlinear RHAs of "Ordinary Standard" bridges.

INTRODUCTION

Current highway bridge design practice in California is governed by the Seismic Design Criteria, SDC-2006 (Caltrans, 2006), which allows equivalent static analysis and linear elastic dynamic analysis for estimating

the displacement demands, and pushover analysis for establishing the displacement capacities for "Ordinary Standard" bridges. For a bridge to be considered as an "Ordinary Standard" bridge, (1) the span length should be less than 90 m, (2) the bridge should be constructed with normal weight concrete, (3) foundations must be supported on spread footings, pile caps with piles or pile shafts, and (4) the soil is not susceptible to liquefaction or lateral spreading during strong shaking (Caltrans, 2006). More than 90% of bridges in California are the "Ordinary Standard" bridges (Mark Yashinsky, oral commun.).

For "Ordinary Standard" bridges, analysis methods based on the linear-elastic assumption may be appropriate in regions having low-seismicity. In seismically active regions, near-fault static (surface displacement) and dynamic effects (long-period velocity pulses) may impart significant seismic demand to bridges and drive them into the inelastic range, invalidating the linear-elastic assumption (Goel and Chopra, 2008; Kalkan and Kunnath, 2006). To fully portray the "true" nonlinear behavior of bridges to near-fault ground motions, nonlinear RHA may be required. Nonlinear RHAs utilize a set of ground motions representing hazard environment expected for the structure. When recorded motions do not exist (as is the case for central U.S.) or when high-intensity records are needed (as is the case for San Francisco and Los Angeles), ground motions from other tectonically similar regions need to be selected and modified. Most of the procedures to modify ground motion records fall into one of two categories: spectral matching (Lilhanand and Tseng, 1987, 1988) and amplitude scaling (Katsanos et al., 2009).

The objective of amplitude-scaling methods is to determine scale factors for a small number of records such that the scaled records provide an accurate estimate of "true" median structural responses, and, at the same time, are efficient (i.e., reduce the record-to-record variability of responses). Amplitude-scaling of records was accomplished previously by scaling them to a common intensity measure, such as peak ground acceleration (PGA), effective peak acceleration, Arias intensity, or effective peak velocity (Nau and Hall, 1984; Kurama and Farrow, 2003). These approaches were generally inaccurate and inefficient for structures responding in the inelastic range (Shome and Cornell, 1998; Kurama and Farrow, 2003). Scaling of records to a target value of the elastic spectral acceleration at a fundamental period provides improved results for structures whose response is dominated by their first-"mode" (Shome et al., 1998). However, this scaling method becomes less accurate and less efficient for structures responding significantly in their higher vibration modes or far into the inelastic range (Mehanny, 1999; Alavi and Krawinkler, 2000; Kurama and Farrow, 2003). To consider higher mode response, a vector intensity measure (IM) of first-"mode" spectral acceleration and the spectral ratio of first-"mode" and second"-mode" have been developed

(Bazzurro, 1998; Shome and Cornell, 1999). Although this vector IM improves accuracy, it remains inefficient for near-fault records with a dominant velocity pulse (Baker and Cornell, 2006).

To recognize the lengthening of the apparent period of vibration due to yielding of the structure, scalar IMs have been considered (Mehanny 1999; Cordova et al., 2000). Alternatively, scaling earthquake records to minimize the difference between its elastic response spectrum and the target spectrum has been proposed (Kennedy et al., 1984; Malhotra, 2003; Alavi and Krawinkler, 2004; Naeim et al., 2004; Youngs et al., 2007). Additional studies have suggested that selection of ground motion records taking into account the elastic spectral shape may provide improved estimates of EDPs (Baker and Cornell, 2005; Mackie and Stajadinovic, 2007). The measure of spectral shape used in these studies is "epsilon", or the number of standard deviations the response spectral ordinate differentiates from a predicted median spectral value from an empirical ground motion prediction equation.

Because the preceding methods do not consider explicitly the inelastic behavior of the structure, they may not be appropriate for near-fault sites where the inelastic deformation can be significantly larger than the deformation of the corresponding linear system. For such sites, scaling methods that are based on the inelastic deformation spectrum or consider the response of the first-"mode" inelastic SDF system are more appropriate (Shantz, 2006; Luco and Cornell, 2007; Tothong and Cornell, 2008; PEER, 2009).

Kalkan and Chopra (2010, 2011a) used these concepts to develop a modal-pushover-based scaling (MPS) procedure for selecting and scaling earthquake ground motion records in a form convenient for evaluating existing structures and proposed designs of new structures. This procedure explicitly considers structural strength, determined from the first-"mode" pushover curve, and determines a scaling factor for each record to match a target value of the deformation of the first-"mode" inelastic SDF system. The MPS procedure for one component of ground motion has been extended for two horizontal components of ground motion for three-dimensional analysis of structural systems (Reyes and Chopra, 2011). The MPS procedure has been proven to be accurate and efficient for low-, medium-, and high-rise symmetric plan buildings (Kalkan and Chopra, 2010, 2011a,b; Reyes and Chopra, 2011). Here, the accuracy and efficiency of the MPS procedure are further evaluated for one and two components of ground motion by applying it to four existing reinforced concrete "Ordinary Standard" bridges typical of reinforced concrete bridge construction in California. These bridges are single-bent overpass, multi-span bridge, curved bridge and skew bridge responding predominantly in their first-"mode".

MPS PROCEDURE FOR "ORDINARY STANDARD" BRIDGES

The existing MPS procedure, for a single horizontal component of ground motion, scales each record by a factor such that the deformation of the first-"mode" inelastic SDF system—established from the first-"mode" pushover curve for the structure due to the scaled record matches a target value of inelastic deformation (Kalkan and Chopra, 2010, 2011a). The target value of inelastic deformation is defined as the median deformation of the first-"mode" inelastic SDF system due to a large ensemble of unscaled ground motions compatible with the site-specific seismic hazard conditions. The target value of inelastic deformation may be estimated by either (1) performing nonlinear RHA of the inelastic SDF system to obtain the peak deformation due to each ground motion, and then computing the median of the resulting data set; or (2) multiplying the median peak deformation of the corresponding linear SDF system, known from the elastic design spectrum (or uniform hazard spectrum) by the inelastic deformation ratio, estimated from an empirical equation with known yield-strength reduction factor.

For first-"mode" dominated structures, scaling earthquake records to the same target value of the inelastic deformation of the first-"mode" SDF system is shown to be sufficient (Kalkan and Chopra, 2010, 2011a).

Summarized below is the step-by-step MPS procedure for "Ordinary Standard" bridges:

1. For the given site, define the target pseudo-acceleration response spectrum either as the probabilistic seismic hazard analysis (PSHA) based uniform hazard spectrum or code-based design spectrum, or the median pseudo-acceleration spectrum for a large ensemble of (unscaled) earthquake records compatible with the site-specific seismic hazard conditions. For California, a web-based tool (http://dap3.dot.ca.gov/shake_stable/index.php) is available to calculate both deterministic and probabilistic design spectrum based on the SDC-2006.

2. Compute the frequencies ω_n (periods T_n) and mode shape vectors $\boldsymbol{\phi}_n$ of the first few modes of elastic vibration of the bridge.

3. Develop the base shear deck displacement V_{b1}-u_{d1} relation or pushover curve by nonlinear pushover analysis of the bridge subjected to gradually increasing lateral forces with an invariant force distribution. The distribution of lateral forces ($\mathbf{s}_n$) is determined from the shape of the

fundamental mode multiplied by tributary mass (lumped mass), that is $\mathbf{s_n} = \mathbf{m}\boldsymbol{\phi}_n$. Gravity loads are applied before starting the pushover analysis.

4. Idealize the pushover curve and select a hysteretic model for cyclic deformations, both appropriate for the bridge's structural system and materials (Han and Chopra, 2006; Bobadilla and Chopra, 2007). Determine the yield-strength reduction factor R_y (equals to strength required for the bridge to remain elastic divided by the yield strength of the structure) from: $R_y = M_1^* \overline{A}_1 / V_{b1y}$, where M_1^* is the effective modal mass, $\overline{A}_1$ is the target spectral acceleration (or design acceleration) at the first-"mode" and V_{b1y} is the yield point value of base shear determined from the idealized pushover curve.

5. Convert the idealized pushover curve to the force-deformation ($F_{s1}/L_1 - D_1$) relation of the first-"mode" inelastic SDF system by utilizing $F_{s1}/L_1 = V_{b1} / M_1^*$ and $D_1 = u_{d1} / (\Gamma_1 \Phi_{d1})$ in which $L_1 = \phi_1 \mathbf{m} \iota$, Φ_{d1} is the value of ϕ_1 at the deck level, u_{d1} is the deck displacement of a bridge under first-"mode" pushover, $\Gamma_1 = (\phi_1' \mathbf{m} \iota) / (\phi_1' \mathbf{m} \phi_1)$ and each element of the influence vector ι is equal to unity (F_{s1}/L_1 v's D_1 is simply the Acceleration Displacement Response Spectrum (ADRS) format).

6. For the first-"mode" inelastic SDF system, establish the target value of deformation $\overline{D}_1^I$ from $\overline{D}_1^I = C_R \overline{D}_1$, where $\overline{D}_1 = (T_1/2\pi)^2 \overline{A}_1$; C_R is determined from an empirical equation (e.g., Chopra and Chintanapakdee, 2003, 2004) for the inelastic deformation ratio corresponding to the yield-strength reduction factor R_y, determined in Step 4 as:

$$C_R = 1 + \left[(L_R - 1)^{-1} + \left(\frac{a}{R_y^b} + c \right) \left(\frac{T_1}{T_c} \right)^d \right]^{-1} \tag{1}$$

in which, the limiting value of C_R at $T_n = 0$ is given by L_R as:

$$L_R = \frac{1}{R_y} \left(1 + \frac{R_y - 1}{\alpha} \right) \tag{2}$$

where *a* is the post-yield stiffness ratio of the inelastic SDF system and T_c is the period separating the acceleration and velocity-sensitive regions of the target spectrum (e.g., see right panel in figure 1); the parameters in equation (1) are: a=61, b=2.4, c=1.5, and d=2.4. Equations (1) and (2) and values of their parameters are valid for far-fault ground motions, independent of (i) earthquake magnitude and distance, and (ii) NEHRP site class B, C, and D; and also for near-fault ground motions.

7. Compute the peak deformation $D_1^I = \max\left|D_1(t)\right|$ of the first-"mode" inelastic SDF system defined by the force deformation relation developed in Steps 4 and 5 and damping ratio ζ_1. The initial elastic vibration period of the system is $T_1 = 2\pi\,(L_1 D_{1y} / F_{s1y})^{1/2}$. For a SDF system with known T_1 and ζ_1, D_1^I can be computed by nonlinear RHA due to one of the selected ground motions $\ddot{u}_g(t)$ multiplied by a scale factor *SF*, to be determined to satisfy Step 8, by solving

$$\ddot{D}_1 + 2\zeta_1\omega_1\dot{D}_1 + F_{s1}D_1 / L_1 = -(SF)\ddot{u}_g(t) \tag{3}$$

8. Compare the normalized difference between the target value of the deformation $\bar{D}_1^I$ of the first-"mode" inelastic SDF system (Step 6) and the peak deformation D_1^I, determined in Step 7 against a specified tolerance, ε

$$\Delta_1 = \left|\bar{D}_1^I - D_1^I\right| / \bar{D}_1^I < \varepsilon \tag{4}$$

9. Determine the scale factor *SF* such that the scaled record $(SF)\ddot{u}_g(t)$ satisfies the criterion of equation (4). Because equation (3) is nonlinear, *SF* cannot be determined *a priori*, but requires an iterative procedure starting with an initial guess. Starting with *SF* = 1, Steps 7 and 8 are implemented and repeated with modified values of *SF* until equation (4) is satisfied. Successive values of *SF* are chosen by trial and error or by a convergence algorithm, for example, quasi Newton iteration procedures (Nocedal and Stephen, 2006). For a given ground motion, if equation (4) is satisfied by more than one *SF*, the *SF* closest to unity should be taken. The rationale behind this is that the applied *SF* should be limited to ensure that the scaled record does not show characteristics that would be unrealistic for the magnitude and distance pair to which it is referred.

Repeat Steps 7 and 8 for as many records as deemed necessary to obtain the scale factors *SF* for a single horizontal component of ground motion. If the structure is analyzed for bi-directional excitations, repeat Steps 1 through 6 to obtain a different target spectrum, pushover curve and SDF properties for the second horizontal component of ground motion. Using these items, specific to each horizontal component of ground motion, repeat Steps 7 and 8 for as many records as deemed necessary to obtain the scale factors. Note that the scale factors will be different for each record and different for each component of ground motion (Reyes and Chopra, 2011). This is the extended MPS procedure for two horizontal components of ground motion.

If the higher modes are important for a given bridge, MPS procedure checks for second-"mode" compatibility of each scaled record by comparing its elastic spectral displacement response values at the second-"mode" vibration period of the bridge against the target spectrum. This approach ensures that each scaled earthquake record satisfies two requirements: (1) the peak deformation of the first-"mode" inelastic SDF system is close enough to the target value of its inelastic deformation; and (2) the peak deformation of the second-"mode" elastic SDF system is not far from the target spectrum. Ground motion records satisfying these two criteria should be used in nonlinear RHA. Further details on higher mode consideration in MPS can be found in Kalkan and Chopra (2010, 2011a,b) and Reyes and Chopra (2011).

GROUND MOTIONS SELECTED

A total of twenty-one near-fault strong earthquake ground motions were compiled from the Next Generation Attenuation project ground motion database. These motions were recorded during seismic events with moment magnitude $6.5 \leq M \leq 7.6$ at closest fault distances $R_{cl} \leq 12$ km and belonging to NEHRP site classification C or D. The twenty-one ground motions, listed in Table 1, are the most intense records available in the NGA database considering the hazard conditions specified. Shown in figure 1 (top panels) are the 5% damped response spectra of the y-component (corresponding to transverse direction of the bridge models) of ground motions. The median spectrum is taken as the design spectrum for purposes of evaluating the MPS procedure; also shown in this figure is the median spectrum of the ground motion ensemble as a four-way logarithmic plot, together with its idealized version (dashed-line). Similarly, the response spectra corresponding to the x-component (corresponding to longitudinal direction of the bridge models) of ground motions are shown in figure 1 (bottom panels). For a particular direction, the idealized spectrum is divided into three period ranges: the long-period region to the right of point *d*, $T_n > T_d$, is called the displacement-sensitive region; the short-period region to the left of point *c*, $T_n < T_c$, is called the

acceleration-sensitive region; and the intermediate-period region between points *c* and *d*, $T_c < T_n < T_d$, is called the velocity-sensitive region (Chopra, 2007; Section 6.8). Note that the nearly constant velocity region is unusually narrow, which is typical of near-fault ground motions.

For the single-bent overpass and multi-span bridge, only the y-component of ground motion was taken into consideration for the analyses. For the curved bridge and the skew bridge, both horizontal components of the twenty-one ground motion records were utilized. Because the twenty-one ground motions selected were not intense enough to drive the curved bridge model far into the inelastic range—an obvious requirement to test any scaling procedure—both horizontal components of the twenty-one ground motions were amplified by a factor of 3. These amplified records were treated as "unscaled" records.

DESCRIPTION OF BRIDGES AND COMPUTER MODELS

In order to cover a wide variety of reinforced concrete bridges, four types of existing "Ordinary Standard" bridges in California were considered: single-bent overpass, multi-span bridge, curved bridge and skew bridge. These bridges and their computer models are introduced briefly below. Their photos, structural drawings, material properties and the details of their computer models in OpenSees (2009) can be found in Kalkan and Kwong (2010).

SINGLE-BENT OVERPASS

The selected bridge with a two-span continuous deck and single-bent composed of two octagonal columns is representative of an overcrossing designed according to post-Northridge Caltrans specifications. The bridge has stub wall abutments restrained in the longitudinal and transverse directions as a result of end diaphragm and wing wall interaction with the soil. The column bent footings were modeled as translational springs in each orthogonal direction. The abutments were modeled as restrained supports in the vertical direction and as translational springs in longitudinal and transverse directions. The finite element model of the bridge is represented by 3-D frame elements passing through the mid-depth of the superstructure and 3-D frame elements passing through the geometric centre and mid-depth of the columns and the cap beam (Figure 2a). Fiber-discretized, force-based nonlinear beam-column elements were used to model columns; the integration along the element is based on Gauss-Lobatto quadrature rule. A fiber section model at each integration point, which in turn is associated with uniaxial material models and enforces the Bernoulli beam assumption for axial force and bending, represents the force-based element. Centerline dimensions were used in the element modeling for all cases. The deck elements were assumed to remain elastic based on

the capacity design approach employed by the SDC-2006. The box-girder was assumed to be integral with the bent, thus full continuity was employed at the superstructure-bent connection. P-Δ effects were considered at the global level.

MULTI-SPAN BRIDGE

The bridge selected is representative of typical multi-span, single-frame prestressed concrete bridges built according to post-Northridge Caltrans design specifications. The bridge was modeled as an elastic superstructure sitting on nonlinear columns on elastic foundation (figure 2b). Fiber-discretized, force-based nonlinear beam-column elements were used to model the columns while the deck elements were assumed to remain elastic. P-Δ effects were considered at the global level. The columns of the bridge rest on shallow foundations. Elastic springs in three translational directions were used to model the soil effect. Seat type abutments are used at both ends of the bridge. Spring systems were used to model the dynamic stiffness of the abutments. In the vertical direction, the movement of the bridge is vertically prevented at the abutments.

CURVED BRIDGE

The curved bridge is representative of typical short-span prestressed concrete bridges built according to post-Northridge Caltrans design specifications. Two columns support the curved deck. Sliding bearings support the bridge at the abutments. The deck was assumed to be elastic while the two columns were modeled as fiber-discretized force-based nonlinear beam-column elements. Due to the curved nature of the deck, the co-rotational geometric transformation was employed for all elements of the model. Co-rotational coordinate transformation performs a near-exact geometric transformation of element stiffness and resisting force from the basic system to the global coordinate system. This approach provides more accurate results than the conventional geometric transformation for large deformations due to P-Δ effects. In terms of boundary conditions, the bases of the two columns were fixed, and the two abutments were modeled as elastic springs.

SKEW BRIDGE

The bridge selected is representative of typical short-span, concrete overcrossings built in late 70s. The “skewed” single bent is roughly near the middle of the span. Wing walls at the abutments support the bridge. In the computer model, the deck was assumed to be elastic while the bent was modeled with two fiber-discretized nonlinear force-based beam-column elements joined by two elastic rigid beams. Due to the

unsymmetrical plan, the co-rotational geometric transformation was employed for all elements of the model. As for the boundary conditions, the bases of the two columns at the bent were fixed. The two abutments, however, were fixed in all degrees of freedom except for the translation along the longitudinal direction and the rotation about the axis parallel to the transverse direction of the bridge. Additionally, one of the abutments was free to move transversely relative to the other abutment.

FIRST – "MODE" SDF-SYSTEM PARAMETERS

The mode shapes of all bridges are provided in Kalkan and Kwong (2010). For the single-bent overpass, the first-"mode" (0.54 s) involves a transverse translation of the deck and the second-"mode" (0.52 s) involves a longitudinal translation of the superstructure. The multi-span bridge has the first-"mode" (2.47 s) in the translational direction and second-"mode" (1.06 s) in the longitudinal direction. The transverse direction is more flexible for both bridges.

For the curved bridge, the first-"mode" (0.41 s) and second-"mode" (0.34 s) involves translation in both the transverse and longitudinal directions of the bridge. Due to the unsymmetrical nature of the bridge, the transverse and longitudinal directions are coupled. For the skew bridge, the first-"mode" (0.81 s) involves primarily translation in the longitudinal direction of the bridge with slight movement in the transverse direction due to skewness while the second-"mode" (0.51 s) consists primarily of translation in the bridge's transverse direction.

Modal pushover curves for four bridges were developed in the transverse and longitudinal directions separately. Similar to the modal pushover analyses procedure for buildings (Chopra, 2007), the distribution of lateral forces was determined from the shape of the fundamental transverse mode, and fundamental longitudinal mode, multiplied by tributary mass (i.e., lumped mass). For the curved and skew bridges, the fundamental mode of the entire 3-D structure was used in determination of the distribution of lateral forces. The pushover curves were then converted to those corresponding to the equivalent SDF system using relations described in Step 5 of the summary of the MPS procedure. For each direction, the resultant SDF pushover curves are displayed in figures 3 and 4 with a thick solid line, while bilinear idealization of pushover curves is shown in thick dashed lines. These stable bilinear curves also define the hysteretic force-deformation relations for each bridge. Since stiffness and strength degradation were not accounted for, the unloading branch of the hysteretic curve has the same slope with that of the initial loading branch.

EVALUATION OF MPS PROCEDURE

The accuracy of the MPS procedure was evaluated by comparing the median (defined as the geometric mean by assuming log-normal distribution of EDP) value of an EDP due to three sets of randomly selected seven scaled ground motions against the benchmark value, defined as the median value of the EDP due to the twenty-one unscaled ground motions. Although the selection process was random, no more than two records from the same event were included in a single set so that no single event is dominant within a set. The use of seven ground motions within a set has been shown to provide statistically robust estimates from nonlinear RHAs (Reyes and Kalkan, 2011).

In evaluation, a scaling procedure is considered to be accurate if the median values of an EDP due to the seven scaled ground motions are close to benchmark value; it is considered to be efficient if the dispersion of an EDP due to the set of seven scaled ground motions is small. Smaller dispersion in EDPs means a smaller number of analyses to obtain a given confidence level in the results. The median value ($\hat{x}$) defined as the geometric mean and the dispersion measure (δ) of *n* observed values of x_i are calculated from the following expressions

$$\hat{x} = \exp\left[\frac{\sum_{i=1}^{n} \ln x_i}{n}\right] \quad \text{and} \quad \delta = \left[\frac{\sum_{i=1}^{n} (\ln x_i - \ln \ddot{o})^2}{n-1}\right]^{1/2} \tag{5}$$

BENCHMARK RESULTS

Figure 5 shows the benchmark EDPs for both the single-bent overpass and multi-span bridge together with results from individual records to show the large record-to-record variability (i.e., large dispersion). EDPs adopted here are global response parameters: peak value of deck drift ratio (i.e., deck displacement ÷ height of column) and maximum column plastic rotation over the response histories. Only the EDP's in the transverse direction were taken into consideration because it is the weakest direction for both bridges. The peak values of deck drift ratios due to the twenty-one unscaled ground motions range from 1% to 5%, and column plastic deformations range from less than 0.01 rad to over 0.05 rad. All of the excitations drive both bridges well into the inelastic range (Kalkan and Kwong, 2010).

Figure 6 shows the benchmark EDPs in the transverse direction (top panels) and in the longitudinal direction (bottom panels) for the curved bridge, along with results from individual records to show the large

record-to-record variability. With a curved span, the terms 'longitudinal' and 'transverse' refer to the global x and y axes, respectively, that are adopted in the OpenSees model. The local axes for the columns are not in alignment with the global axes. Consequently, the column plastic rotations, recorded with respect to the local axes, are not in alignment with the global axes. The peak drift ratios, however, are determined with respect to global axes. Nevertheless, the column plastic rotations associated with the local axes are still referred to as transverse and longitudinal EDPs. It can be seen in figure 6 that EDPs in the transverse direction are generally larger than those in the longitudinal direction. For peak drift ratios, the median value is 1.5% in the transverse direction whereas the median value is 0.85% in the longitudinal direction. Similarly, for column plastic rotations, the median is 0.005 rad in the transverse direction whereas the median is 0.002 rad in the longitudinal direction.

Figure 7 shows the benchmark EDPs in the transverse direction (top panels) and in the longitudinal direction (bottom panels) for the skew bridge. Due to the boundary conditions for this model, the EDPs in the longitudinal direction are generally much larger than those in the transverse direction. For peak drift ratios, values in the transverse direction ranged from 0.5% to slightly over 1%, with a median value of 0.63%, while those in the longitudinal direction ranged from 1% to over 6%, with a median value of 2.5%. Similarly, for column plastic rotations, values in the transverse direction ranged from 0.002 rad to about 0.01 rad, with a median value of 0.005 rad, while those in the longitudinal direction ranged from 0.01 rad to over 0.06 rad, with a median value of 0.023 rad. All of the excitations led to inelastic responses for both curved and skew bridges (Kalkan and Kwong, 2010).

TARGET VALUE OF INELASTIC DEFORMATION

In evaluation of the MPS procedure, "exact" target value of inelastic deformation $\bar{D}_1'$ was assumed to be unknown, and it was estimated (Step 6 of the MPS procedure) by the C_R equation (Chopra and Chintanapakdee, 2003, 2004) using post-yield stiffness ratio (figures 3 and 4) and yield-strength ratio. Yield-strength ratio R_y was determined (Step 4 of the MPS procedure) as 3.1 and 3.5, respectively for the single-bent overpass and multi-span bridge. Alternatively, "exact*" target value of deformation $\bar{D}_1'$ was computed by nonlinear RHAs of the first-"mode" inelastic SDF system for twenty-one unscaled records. Figure 8 compares the estimated target value of deformation using the C_R equation against its "exact"

* The term "exact" is used herein a somewhat loose sense as implied by the quotation mark because it is defined on the basis of twenty-one ground motions. According to the random sampling theory, this set is assumed to be a representative subset of a much larger population of recorded and not yet recorded ground motions according to the specified hazard conditions.

value for the single-bent overpass and multi-span bridge; values from individual records are also included to show its large record-to-record variability. In this figure, the C_R equation overestimates "exact" value of $\bar{D}_1^I$ by 12%-14%.

For the curved and skew bridges, which will be analyzed under bi-directional excitations due to their irregular geometry, the MPS procedure will be applied to each horizontal direction separately. This requires consideration of target deformation in both horizontal directions (Reyes and Chopra, 2011). Figure 9 (top panels) compares the estimated target value using the C_R equation against its "exact" value for both the y and x components of ground motion for the curved bridge. The yield-strength ratio used in the C_R equation was determined as 1.61 for the y direction. The C_R value for the x direction is set to 1 because the force required for the SDF system, in this particular direction, to remain elastic is less than its yield force. Figure 9 (bottom row) compares the estimated target value using the C_R equation against its "exact" value for both the y and x components of ground motion for the skew bridge. The yield-strength ratios were determined as 6.1 and 2 for the x and y directions, respectively. It is observed that the target value of inelastic deformation $\bar{D}_1^I$ is much greater in the longitudinal direction than that in the transverse direction. For these two bridge models, the C_R equation overestimates the "exact" value of $\bar{D}_1^I$ by 9%-18% in the transverse direction and by 1%-3% in the longitudinal direction.

COMPARISONS AGAINST BENCHMARK RESULTS

Both the single-bent overpass and multi-span bridge are first-"mode" dominated; the modal participation ratio for the first-"mode" is much larger than other higher modes. Thus, Steps 7 and 8 of the single-component MPS procedure are implemented to determine an appropriate scale factor for each record. In the curved and skew bridge models, the two-component MPS procedure (Reyes and Chopra, 2011) is implemented to determine an appropriate scale factor for each horizontal component of each record. The scale factors established for all bridges are less than 3 indicating that the original characteristics of the ground motions are in general well retained. The values of scale factors for each bridge and for each set are reported in Kalkan and Kwong (2010).

The EDPs determined by nonlinear RHAs of bridges due to three sets of 7 ground motions scaled according to the MPS procedure are compared first against the benchmark EDPs. Figures 10-17 exhibit the

representative comparisons for the transverse EDPs. Reader may refer to Kalkan and Kwong (2010) for the complete sets of comparisons.

To better examine the accuracy of the MPS procedure, ratios of median value of EDPs from the MPS procedure to the benchmark value are computed and listed in Table 2 for each bridge and for each set of ground motions. For the single-bent overpass (figure 10), the maximum deviation of median value of EDPs due to the MPS procedure from the benchmark value is 18% for the deck drift ratio and 21% for the column plastic rotation for Set 1. More accurate results with deviations ranging from 7%-10% were obtained in case of Sets 2 and 3. For the multi-span bridge (figure 11), median deck drift ratios due to the MPS procedure overestimate the benchmark value by a maximum of 14% for deck drift ratio and 19% for column plastic rotation in Set 2. Using Sets 1 and 3 resulted in slightly better accuracy, with the deviations in the range of 10%-17%. For the curved bridge (figure 12), the median values of deck drift ratios are greater than the benchmark values by 38% on average in the transverse direction (see Table 2). In the case of the skew bridge model (figure 13), the median values of deck drift ratios are larger than the benchmark values by 30% on average in the transverse direction. The column plastic rotations are, on average, 33% greater in the transverse direction.

As evident in figures 10 through 13, the dispersion of EDPs is significantly reduced when records are scaled using the MPS procedures (compare with larger scatter from figures 5, 6 and 7). To quantify this reduction, the standard deviation (δ, see equation 5) of ratio of the EDP value from each individual ground motion to the median benchmark value is computed and listed in Table 3 for each set of ground motions and for each bridge. It is apparent in this table that the dispersion in each set and for each bridge is much lower than that from the corresponding benchmark cases, where records are unscaled but consistent with the hazard condition defined in terms of magnitude, distance and site-condition.

For the single-bent overpass, the standard deviations (δ) of EDPs from the unscaled records are reduced by 39% to 77% using the one-component MPS procedure. For the multi-span bridge, the reduction in δ is in the range of 33% to 66%. These results demonstrate that the one-component MPS procedure leads to scaled ground motions that yield accurate estimates of median EDPs that are accompanied with dramatically reduced dispersions relative to the unscaled ground motions, as well.

With regard to the curved bridge, the reduction in δ for the EDPs is, on average, 50% for the transverse direction and 39% for the longitudinal direction. For the skew bridge, the reduction in δ for the EDPs is, on average, 60% for the transverse direction, and 54% for the longitudinal direction. These results

demonstrate that scaling records with the two-component MPS procedure provides EDPs with dispersion that is significantly lower than that obtained with unscaled ground motions.

Utilizing the “exact” value of the target inelastic deformation (i.e., median inelastic deformation value as shown in figure 8), in the one-component MPS procedure (referred to as MPS-“Exact”) further improves the accuracy as shown in figures 14 and 15 for the single-bent overpass and multi-span bridge, respectively. For the single-bent overpass, the maximum deviation of median EDPs due to the MPS-“Exact” procedure from the benchmark value is 15% for the deck drift ratio and 16% for the column plastic rotation considering Set-2. Much better accuracy is obtained using Set 1, and excellent agreement with the benchmark values is achieved using Set 3. For the multi-span bridge, median values of EDPs due to the three sets of ground motions perfectly match with the benchmark values (maximum deviation is only 6%).

Utilizing the “exact” value of the target inelastic deformation in both horizontal directions of ground motion (i.e., median inelastic deformation value as shown in figure 9), in the two-component MPS procedure (referred to as MPS-“Exact”) also further improves the accuracy as shown in figures 16 and 17 for the curved and skew bridges. From the figures (plotted in the same scales), it is evident that the median value from each set is much closer to the benchmark value.

Referring to Table 2 for the curved bridge, the peak drift ratios are now only about 19% larger in the transverse direction and 18% larger in the longitudinal direction than the benchmark value. Similarly, the column plastic rotations are on average, 56% larger in the transverse direction and 55% larger in the longitudinal direction than the benchmark plastic rotations.

A similar improvement in accuracy is also observed for the skew bridge model as shown in Table 2. The peak drift ratios are, on average, 19% larger in the transverse direction and, on average, 23% larger in the longitudinal direction than the benchmark drift ratio. The column plastic rotations are now roughly 21% greater in both directions than the benchmark plastic rotations. Similar to the curved bridge model, the discrepancies are alike in magnitude for both directions.

As shown in Table 3 for the multi-span bridge, the dispersion in EDPs is also further reduced (12%, on average, as compared to the MPS procedure) by utilizing the “exact” value of the target inelastic deformation for the one-component MPS procedure. A less reduction in dispersion (3% on average) is observed in the single-bent overpass. Similarly, the dispersion in EDPs further diminished for the skew and curved bridges by utilizing the “exact” values of the target inelastic deformation in both directions for the two-component MPS procedure. This reduction is 5% for the skew bridge and 4% for the curved bridge.

How will these results change if a different combination of seven ground motions was used? In order to answer this question systematically, the ratio of median EDP value from a set of seven records to benchmark value (EDP value ÷ benchmark value) was computed for as many sets of ground motions as possible. With 21 records to choose from and 7 records used in a single set, 116,280 sets were constructed. With over 100,000 possible realizations of the EDP ratios, histograms may be plotted. The distributions of median EDP ratios for deck drift and column plastic rotation are shown in figure 18 (based on the MPS-"Exact" approach) for the single-bent overpass and multi-span bridge. The median results from the original randomly selected three sets of seven records (Sets 1 through 3) are also presented. It is evident that the results based on arbitrary Sets 1 through 3 lie within the 16- and 84-percentile range of the overall distribution of deck drift ratio, where the median and standard deviation for this distribution are 0.98 and 0.08 respectively. For the multi-span bridge, the results from the three randomly selected sets also cover the 16- and 84-percentile for deck drift ratio distribution with a median and a standard deviation of 1.02 and 0.05, respectively. Similar observations can be made for the plastic rotation response quantity. In all, this figure indicates that the results from the randomly selected three sets (Sets 1 through 3) are representative subsets of a much larger population.

CONCLUSIONS

Based on four "Ordinary Standard" bridges in California, the accuracy and efficiency of the MPS procedure (both one and two-component versions) are assessed by comparing the median values of the engineering demand parameters (EDPs) due to three sets of seven scaled records against the benchmark values. The one-component MPS procedure was applied to the single-bent overpass and multi-span bridge while the two-component MPS procedure was applied to the curved and skew bridges. The efficiency of the MPS scaling procedure was evaluated by computing the dispersion of the responses to the seven scaled ground motions in each set and comparing it with that from the benchmark cases. This evaluation of the MPS procedures has led to the following conclusions:

1. Even for the most intense near-fault ground motions, which represent severe tests, the one-component MPS method with a small number of records estimates the median value of seismic demands to a good degree of accuracy for bridges having regular geometry. The maximum discrepancy is 18% of the benchmark value for the single-bent overpass and 14% of the benchmark value for the multi-span bridge. The average discrepancies of 12% in deck drift ratios and 14% in

column plastic rotations for both bridges are achieved. This demonstrates the accuracy of the one-component MPS method.

2. Considering bidirectional ground excitation, the two-component MPS procedure overestimates seismic demands for bridges with irregular geometries. For the curved bridge model, the average discrepancies in column plastic rotations are larger than those for peak drift ratios. The average discrepancy for peak drift ratios is 38% in the transverse direction and 33% in the longitudinal direction. For the skew bridge model, however, the average discrepancies for peak drift ratios are smaller, as such 30% in the transverse direction and 26% in the longitudinal direction.

3. The dispersion (or record-to-record variability) in the EDPs due to seven scaled records around the median is much smaller when records are scaled by both the one-component and two-component MPS procedures as compared to the unscaled records. This implies stability in the EDPs estimated from records that are scaled according to the MPS procedures relative to those obtained from unscaled records. Despite high levels of inelastic action and irregular geometries, the MPS procedures can reduce the scatter in estimates by 50% on average. These observations indicate the efficiency of the MPS procedures. It should be noted that smaller dispersion in EDPs means a smaller number of analyses to obtain a given confidence level in the EDPs.

4. Utilizing “exact” target value of inelastic deformation further improves the accuracy but slightly improves the efficiency. This improvement in accuracy depends, however, on the precision involved in estimating the “exact” target value of inelastic deformation. Although the additional reduction in dispersion is about 12% for the multi-span bridge, it is less than 5% for all other bridge models.

As shown here for the “Ordinary Standard” bridges, the MPS procedures were accurate and efficient enough in reducing the number of records needed to provide stable estimates of peak displacement and plastic rotation demands from nonlinear RHA of geometrically regular bridges to levels practical for typical bridge design offices. Due to complex response behavior of geometrically irregular bridges, the MPS-“Exact” procedure utilizing exact value of target inelastic deformation provides more accurate results as compared to the MPS procedure utilizing estimated value of target inelastic deformation. All reported results here are based on stable force-deformation relations. Although not expected, adopting other hysteretic model may alter the results achieved regarding either the accuracy or the efficiency of the procedure.

DATA AND RESOURCES

Readers are referred to the MPS procedure website http://nsmp.wr.usgs.gov/ekalkan/MPS/index.html for further details on assessment of the one- and two-component MPS methods, and also for accessing MatLAB codes for scaling ground motion records using the MPS and MPS-"Exact" methods.

ACKNOWLEDGMENTS

First author would like to acknowledge the generous support of the Earthquake Engineering Research Institute for providing him the 2008 EERI/FEMA NEHRP Professional Fellowship in Earthquake Hazard Reduction to pursue a research study on developing "*Practical Guidelines to Select and Scale Earthquake Records for Nonlinear Response History Analysis of Structures*"; this paper is a sequel to this earlier work. We also wish to acknowledge the insightful comments of Anil K. Chopra and generous support of Sungchil Lee, Maria Feng, Sashi K. Kunnath and Emrah Erduran with OpenSees models. Lastly, thanks to Juan Carlos Reyes, Toorak Zokaie, Farzin Zareian, and two anonymous reviewers for their valuable comments and suggestions, which helped to improve the technical quality of this paper.

REFERENCES

Alavi, B. and Krawinkler, H. (2000). "Consideration of near-fault ground motion effects in seismic design", *Proc. of the Twelfth World Conf. on Eq. Eng*., Paper no. 2665, Auckland, New Zealand.

Baker, J. W. and Cornell, C. A. (2005). "A vector-valued ground motion intensity measure consisting of spectral acceleration and epsilon", *Eq. Eng. and Str. Dyn.*, Vol. 34, no. 10, pp. 1193-1217.

Baker, J. W. and Cornell, A. C. (2006). "Spectral shape, epsilon and record selection," *Eq. Eng. and Str. Dyn.,* Vol. 35, no. 9, pp. 1077-1095.

Bazzurro, P., (1998). Probabilistic Seismic Demand Analysis, Ph.D. thesis, Dept. of Civil and Env. Eng., Stanford University, CA. (Available online at http://www.stanford.edu/group/rms/Thesis/index.html; last accessed on 06/2008).

Bobadilla, H. and A. K. Chopra (2007). Modal Pushover Analysis for Seismic Evaluation of Reinforced Concrete Special Moment Resisting Frame Buildings, Earthquake Engineering Research Center, EERC/2007-01, 68 p.

Caltrans (2006). Seismic Design Criteria: Version 1.4, California Department of Transportation, Sacramento, CA. (http://www.dot.ca.gov)

Chopra, A. K. (2007). Dynamics of Structures: Theory and Applications to Eq. Eng. Prentice Hall, Englewood Cliffs, N.J.

Chopra, A. K. and Chintanapakdee, C. (2003). Inelastic Deformation Ratios for Design and Evaluation of Structures: Single-Degree-of-Freedom Bilinear Systems. Report no. UCB/EERC-2003/09, Earthquake Engineering Research Center, University of California, Berkeley, 67 p.

Chopra, A. K. and Chintanapakdee, C. (2004). "Inelastic Deformation Ratios for Design and Evaluation of Structures: Single-Degree-of-Freedom Bilinear Systems", *J. of Str. Eng*. (ASCE), Vol. 130, no. 9, pp. 1304-1319.

Cordova, P. P., Deierlein, G. G., Mehanny, S. S. F. and Cornell, C. A., (2000). Development of a two-parameter seismic intensity measure and probabilistic assessment procedure, Proceedings of the 2nd U.S.-Japan Workshop on Performance-Based Seismic Design Methodology for Reinforced Concrete Building Structures, PEER Report 2000/10, Pacific Earthquake Engineering Research Center, University of California, Berkeley, CA.

Goel, R.K. and Chopra A.K. (2008). Estimating Seismic Demands For "Ordinary" Bridges Crossing Fault-Rupture Zones, Earthquake Engineering Research Center, University of California at Berkeley, Report no. UCB/EERC-2008/01.

Han, S. W. and Chopra, A. K. (2006). "Approximate Incremental Dynamic Analysis using the Modal Pushover Analysis Procedure", *Eq. Eng. and Str. Dyn*., Vol. 35, pp. 1853-1873.

Kalkan, E. and Kunnath, S. K. (2006). "Effects of Fling-Step and Forward Directivity on the Seismic Response of Buildings", *Earthquake Spectra,* Vol. 22, no. 2, pp. 367-390.

Kalkan, E. and Chopra, A. K. (2010). Practical Guidelines to Select and Scale Earthquake Records for Nonlinear Response History Analysis of Structures, USGS Open File Report No: 2010-1068, 126 p. (Available online at http://pubs.usgs.gov/of/2010/1068/; last accessed on 03/2011).

Kalkan, E., and Chopra, A. K. (2011a). "Modal-Pushover-based Ground Motion Scaling Procedure", *J. of Str. Eng*. (ASCE), Vol. 137, no. 3, pp. 298-310.

Kalkan, E. and Chopra, A. K. (2011b). "Evaluation of Modal Pushover-based Scaling of one Component of Ground Motion: Tall Buildings", *Earthquake Spectra* (in-press; available online at http://nsmp.wr.usgs.gov/ekalkan/PDFs/Papers/J33_Kalkan_Chopra.pdf; last accessed on 03/2011).

Kalkan, E. and Kwong, N. S. (2010). Documentation for Assessment of Modal Pushover-based Scaling Procedure for Nonlinear Response History Analysis of "Ordinary Standard" Bridges: U.S. Geological

Survey Open-File Report 2010-10, p. 56. (Available online at http://pubs.usgs.gov/of/2010/1328/of2010-1328.pdf; last accessed on 03/2011).

Katsanos, E. I., Sextos, A. G. and Manolis, G. D. (2009). "Selection of earthquake ground motion records: A state-of-the-art review from a structural engineering perspective", *Soil Dynamics and Earthquake Engineering*, Vol. 30, no. 4, pp. 157-169.

Kennedy, R. P., Short, S. A., Merz, K. L., Tokarz, F. J., Idriss, I. M., Power, M. S. and Sadigh, K. (1984). "Engineering characterization of ground motion-task 1: Effects of characteristics of free-field motion on structural response", NUREG/CR-3805, U.S. Regulatory Commission, Washington, D.C.

Kurama, Y. and Farrow, K. (2003). "Ground motion scaling methods for different site conditions and structure characteristics", *Eq. Eng. and Str. Dyn.*, Vol. 32, no. 15, pp. 2425-2450.

Lilhanand, K. and Tseng, W. S. (I987). "Generation of synthetic time histories compatible with multiple-damping design response spectra", *Transactions of the 9th International Conf. on Structural Mechanics in Reactor Technology*, Lausanne, K1, 105-110.

Lilhhand, K. and Tseng, W. S. (1988). "Development and application of realistic earthquake time histories compatible with multiple damping design spectra," *Proc. of the Ninth World Conf. on Eq. Eng.*, Tokyo-Kyoto, Japan, Vol. 2, pp. 819-824.

Luco, N. and Cornell, A. C. (2007). "Structure-Specific Scalar Intensity Measures for Near-Source and Ordinary Earthquake Ground Motions", *Earthquake Spectra*, Vol. 23, no. 2, pp. 357–392.

Mackie, K. R. and Stajadinovic, B. (2007). "Three-Dimensional Ground Motion Scaling for Highway Bridges", *Proc. of the 9th Canadian Conf. on Eq. Eng*. Ottawa, Canada, 26-29 June.

Malhotra, P. K. (2003). "Strong-Motion Records for Site-Specific Analysis", *Earthquake Spectra*, Vol. 19, no. 3, pp. 557-578.

Mander, J. B., Priestley M. J. N and Park, R. (1998). "Theoretical stress–strain model for confined concrete", *J. of Str. Eng.*, (ASCE), Vol. 114, no. 8, pp.1804–26.

Mehanny, S. S. F. (1999). Modeling and Assessment of Seismic Performance of Composite Frames with Reinforced Concrete Columns and Steel Beams, Ph.D. thesis, Dept. of Civil and Env. Eng., Stanford University, California.

Naeim, F., Alimoradi, A., and Pezeshk, S. (2004). "Selection and scaling of ground motion time histories for structural design using genetic algorithms," *Earthquake Spectra*, Vol. 20, no. 2, pp. 413-426.

Nau, J. and Hall, W. (1984). "Scaling methods for earthquake response spectra", *J. of Str. Eng*. (ASCE), Vol. 110, no. 91-109.

Nocedal, J., and Stephen J. W. (2006). Numerical Optimization, 2nd ed., Springer Series in Operations Research, Springer, USA.

OpenSees. Open Source finite element platform for earthquake engineering simulations (2009). University of California Berkeley, Pacific Earthquake Engineering Center.

PEER Ground Motion Selection and Modification Working Group, (2009). Evaluation of Ground Motion Selection and Modification Methods: Predicting Median Interstory Drift Response of Buildings, Haselton, C.B. (editor). PEER Report 2009/01, University of California, Berkeley, CA.

Reyes, J. C. and Chopra, A. K. (2011). "Modal Pushover-Based Scaling of Two Components of Ground Motion Records for Nonlinear RHA of Buildings", *Earthquake Spectra*, (in press).

Reyes, J. C. and Kalkan, E. (2011). Required Number of Ground Motion Records for ASCE/SEI 7 Ground Motion Scaling Procedure: U.S. Geological Survey Open-File Report 2011-1, p. 34. (Available online at http://pubs.usgs.gov/of/2010/1328/of2010-1328.pdf; last accessed on 03/2011).

Shantz, T. J. (2006). "Selection and scaling of earthquake records for nonlinear dynamic analysis of first-"mode" dominant bridge structures", *Proc. of the 8th US National Conf. on Eq. Eng.*, San Francisco, CA.

Shome, N. and Cornell, A. C. (1998). "Normalization and scaling accelerograms for nonlinear structural analysis", *Prof. of the Sixth U.S. National Conf. on Eq. Eng.*, Seattle, WA.

Shome, N., Cornell, C. A., Bazzurro, P. and Carballo, J. E., (1998). "Earthquakes, records and nonlinear responses", *Earthquake Spectra*, Vol. 14, no.3, pp. 469–500.

Shome, N. and Cornell, C. A., (1999). Probabilistic Seismic Demand Analysis of Nonlinear Structures, Reliability of Marine Structures Program Report no. RMS-35, Dept. of Civil and Env. Eng., Stanford University, CA.

Tothong, P. and Cornell, A.C. (2008). "Structural performance assessment under near-source pulse-like ground motions using advanced ground motion intensity measures", *Eq. Eng. and Str. Dyn.*, Vol. 37, no. 7, pp. 1013-1037.

Youngs, R. Power, M., Wang, G., Makdisi, F. and Chin, C. C. (2007). "Design Ground Motion Library (DGML) – Tool for Selecting Time History Records for Specific Engineering Applications (Abstract)," SMIP07 Seminar on Utilization of Strong-Motion Data, pp. 109-110.

NOTATION

The following symbols are used in this paper:

$\bar{A}_n$	=	Target pseudo-spectral acceleration
C_R	=	Ratio of peak deformations of inelastic and corresponding elastic SDF systems for systems with known yield-strength reduction factor
$\bar{D}_n$	=	Target value of nth mode elastic deformation
$\bar{D}_1^I$	=	First-"mode" target value of inelastic spectral displacement
$D_n(t)$	=	Deformation of a SDF system
D_1^I	=	Peak deformation of inelastic SDF system
D_n	=	Peak deformation of elastic SDF system
$D_{1,y}$	=	Yield deformation of inelastic SDF system
F_{s1}	=	System resisting force under first-"mode" pushover
$\mathbf{m}$	=	Mass matrix of a MDF system
M	=	Moment magnitude of earthquake
M^*		Effective modal mass
n	=	Mode sequence number
R_y	=	Yield-strength reduction factor
R_{rup}	=	Closest distance to co-seismic rupture plane
$\boldsymbol{s}_n^*$	=	Load vector of modal pushover analysis
SF	=	Ground motion scaling factor
T_n	=	Elastic natural vibration period
T_c	=	Period separating acceleration and velocity-sensitive regions of the spectrum
u_{d1}	=	Deck displacement of a bridge under first-"mode" pushover
$\ddot{u}_g$	=	Earthquake ground acceleration
V_{b1}	=	Base shear under first-"mode" pushover
V_{b1y}	=	Global yield strength under first-"mode" pushover
V_{S30}	=	Average shear-wave velocity within 30 m depth from surface
α	=	Ratio of post-yield and initial stiffness
ζ	=	Damping ratio
Γ	=	Modal participation factor
$\boldsymbol{\phi}$	=	Mode shape vector
$\boldsymbol{\iota}$	=	Influence vector

Table 1. Selected near-fault ground motion records

No.	Earthquake	Year	Station	M	R_{rup} (km)	V_{S30} (m/s)
1	Tabas, Iran	1978	Tabas	7.4	2.1	767
2	Imperial Valley	1979	EC Meloland Overpass FF	6.5	0.1	186
3	Imperial Valley	1979	El Centro Array #7	6.5	0.6	211
4	Superstition Hills	1987	Parachute Test Site	6.5	1.0	349
5	Loma Prieta	1989	LGPC	6.9	3.9	478
6	Erzincan, Turkey	1992	Erzincan	6.7	4.4	275
7	Northridge	1994	Jensen Filter Plant	6.7	5.4	373
8	Northridge	1994	Newhall - W Pico Canyon Rd	6.7	5.5	286
9	Northridge	1994	Rinaldi Receiving Sta	6.7	6.5	282
10	Northridge	1994	Sylmar - Converter Sta	6.7	5.4	251
11	Northridge	1994	Sylmar - Converter Sta East	6.7	5.2	371
12	Northridge	1994	Sylmar - Olive View Med FF	6.7	5.3	441
13	Kobe, Japan	1995	Port Island	6.9	3.3	198
14	Kobe, Japan	1995	Takatori	6.9	1.5	256
15	Kocaeli, Turkey	1999	Yarimca	7.4	4.8	297
16	Chi-Chi, Taiwan	1999	TCU052	7.6	0.7	579
17	Chi-Chi, Taiwan	1999	TCU065	7.6	0.6	306
18	Chi-Chi, Taiwan	1999	TCU068	7.6	0.3	487
19	Chi-Chi, Taiwan	1999	TCU084	7.6	11.2	553
20	Chi-Chi, Taiwan	1999	TCU102	7.6	1.5	714
21	Duzce, Turkey	1999	Duzce	7.2	6.6	276

Table 2. Comparison of EDP ratios considering MPS and MPS-"Exact" for four bridges and for three sets of seven ground motion records

	Single-bent Overpass					
	MPS			MPS-"Exact"		
EDP Ratio (MPS Median ÷ Benchmark)	**Set-1**	**Set-2**	**Set-3**	**Set-1**	**Set-2**	**Set-3**
Deck Drift	1.18	0.93	1.08	1.08	0.85	1.00
Column Plastic Rotation	1.21	0.93	1.10	1.10	0.84	1.01

	Multi-span Bridge					
	MPS			MPS-"Exact"		
EDP Ratio (MPS Median ÷ Benchmark)	**Set-1**	**Set-2**	**Set-3**	**Set-1**	**Set-2**	**Set-3**
Deck Drift	1.12	1.14	1.10	1.04	1.00	1.02
Column Plastic Rotation	1.17	1.19	1.13	1.06	1.00	1.04

	Curved Bridge					
	MPS			MPS-"Exact"		
EDP Ratio (MPS Median ÷ Benchmark)	**Set-1**	**Set-2**	**Set-3**	**Set-1**	**Set-2**	**Set-3**
Deck Drift (Trans)	1.32	1.48	1.35	1.16	1.26	1.14
Column Plastic Rotation (Trans)	1.99	2.25	1.91	1.57	1.74	1.38
Deck Drift (Long)	1.29	1.42	1.29	1.15	1.27	1.12
Column Plastic Rotation (Long)	1.79	2.09	1.67	1.53	1.80	1.32

	Skew Bridge					
	MPS			MPS-"Exact"		
EDP Ratio (MPS Median ÷ Benchmark)	**Set-1**	**Set-2**	**Set-3**	**Set-1**	**Set-2**	**Set-3**
Deck Drift (Trans)	1.34	1.30	1.25	1.22	1.20	1.14
Column Plastic Rotation (Trans)	1.37	1.35	1.28	1.22	1.25	1.15
Deck Drift (Long)	1.20	1.30	1.29	1.14	1.27	1.27
Column Plastic Rotation (Long)	1.24	1.25	1.24	1.17	1.24	1.22

Table 3. Comparison of dispersion measures (δ) considering MPS and MPS-"Exact" for four bridges and for three sets of seven ground motion records

	Single-bent Overpass						
		MPS			MPS-"Exact"		
Dispersion Measure (δ)	Benchmark	Set-1	Set-2	Set-3	Set-1	Set-2	Set-3
Deck Drift	0.52	0.12	0.31	0.22	0.13	0.29	0.21
Column Plastic Rotation	0.56	0.13	0.34	0.24	0.14	0.32	0.23

	Multi-span Bridge						
		MPS			MPS-"Exact"		
Dispersion Measure (δ)	Benchmark	Set-1	Set-2	Set-3	Set-1	Set-2	Set-3
Deck Drift	0.40	0.26	0.21	0.14	0.21	0.17	0.14
Column Plastic Rotation	0.45	0.30	0.27	0.16	0.28	0.22	0.15

	Curved Bridge						
		MPS			MPS-"Exact"		
Dispersion Measure (δ)	Benchmark	Set-1	Set-2	Set-3	Set-1	Set-2	Set-3
Deck Drift (Trans)	0.51	0.29	0.29	0.28	0.29	0.31	0.24
Column Plastic Rotation (Trans)	1.15	0.46	0.46	0.56	0.49	0.47	0.55
Deck Drift (Long)	0.47	0.31	0.31	0.27	0.31	0.29	0.24
Column Plastic Rotation (Long)	1.08	0.60	0.70	0.57	0.54	0.67	0.52

	Skew Bridge						
		MPS			MPS-"Exact"		
Dispersion Measure (δ)	Benchmark	Set-1	Set-2	Set-3	Set-1	Set-2	Set-3
Deck Drift (Trans)	0.47	0.16	0.20	0.19	0.15	0.17	0.17
Column Plastic Rotation (Trans)	0.57	0.30	0.19	0.23	0.27	0.12	0.20
Deck Drift (Long)	0.95	0.47	0.39	0.39	0.47	0.38	0.38
Column Plastic Rotation (Long)	0.71	0.40	0.27	0.33	0.40	0.29	0.32

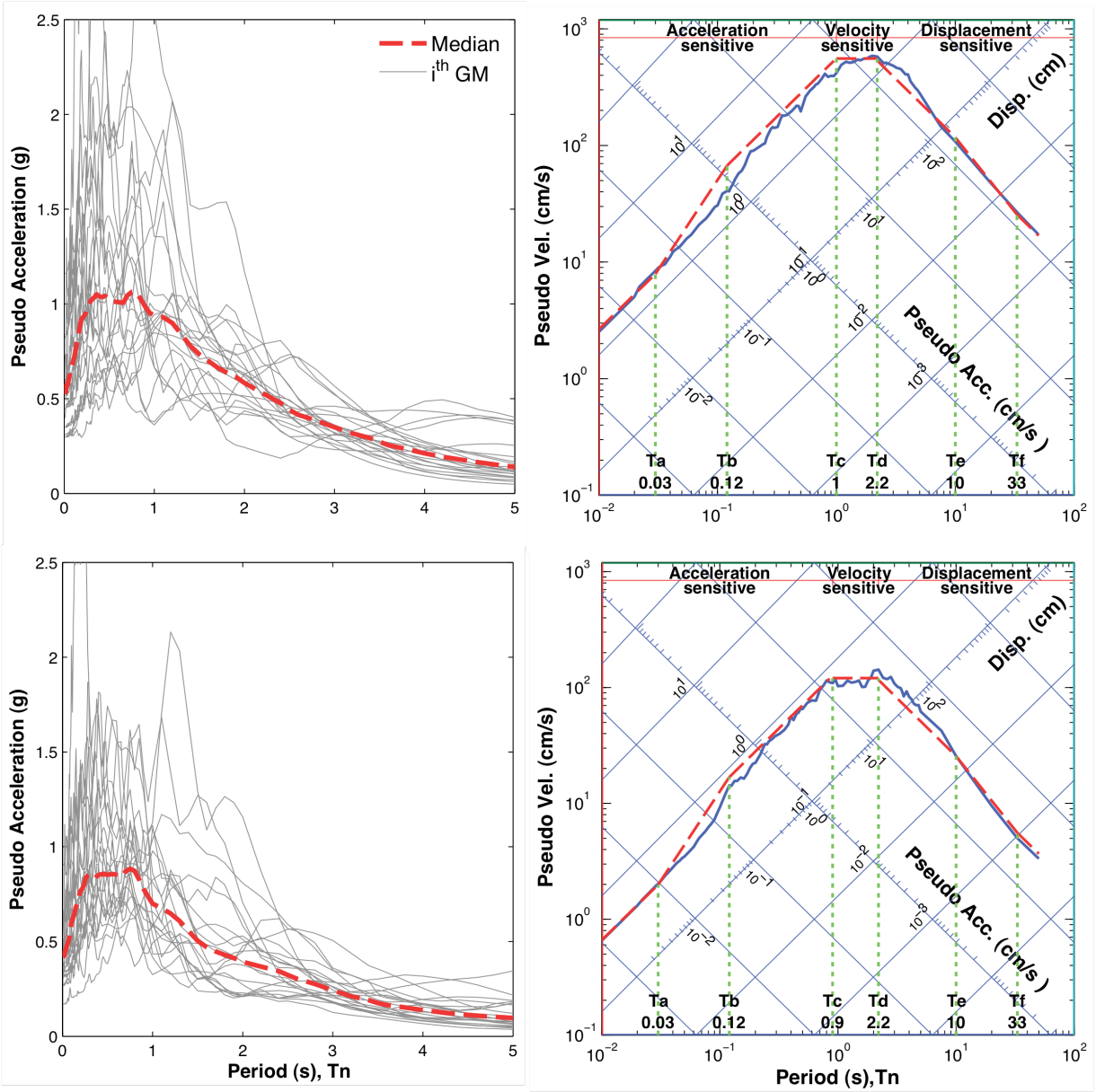

Figure 1. [Left panels] Individual response spectra for twenty-one unscaled ground motions and their median response spectrum taken as the design spectrum; [Right panels] Median elastic response spectrum (i.e., design spectrum) shown by a solid line, together with its idealized version in dashed line; spectral regions are also identified; Damping ratio, ζ = 5%. [Top panels] "y-component" of the ground motion records (i.e., transverse direction of bridge models); [Bottom panels] "x-component" of the ground motion records (i.e., longitudinal direction of bridge models).

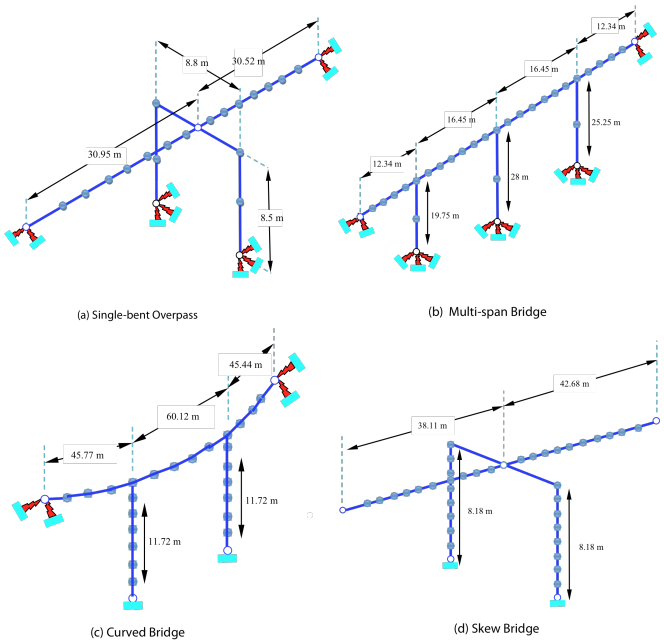

Figure 2. Idealized computer models of bridges.

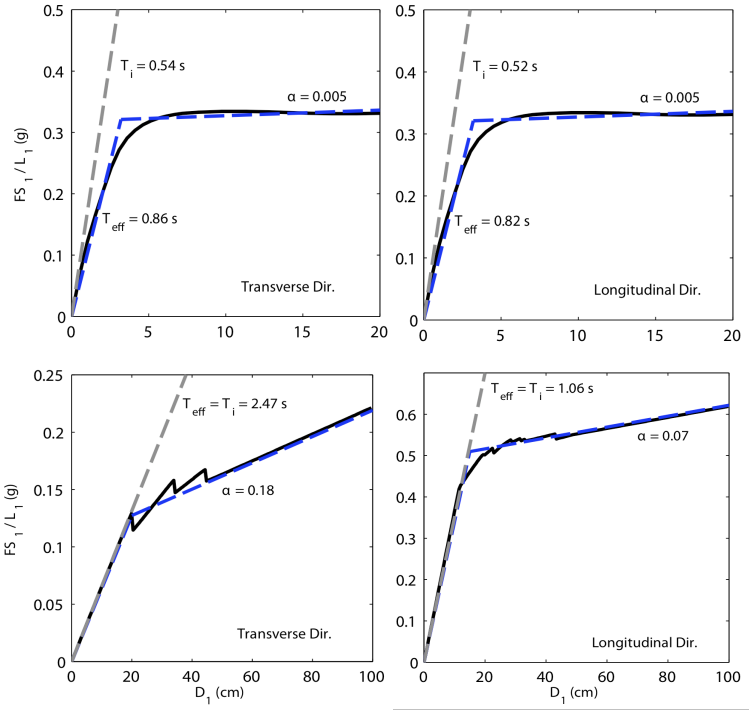

Figure 3. First-"mode" SDF pushover curve (solid line) and its idealized bilinear model (dashed line) in transverse and longitudinal directions for single-bent overpass [top panels] and multi-span bridge [bottom panels].

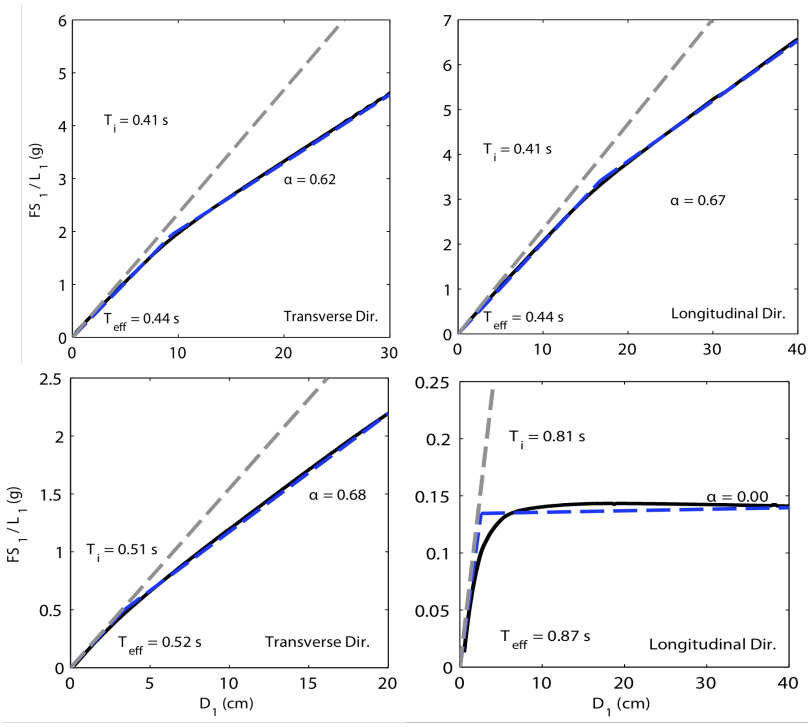

Figure 4. First-"mode" SDF pushover curve (solid line) and its idealized bilinear model (dashed line) in transverse and longitudinal directions for curved bridge [top panels] and skew bridge [bottom panels].

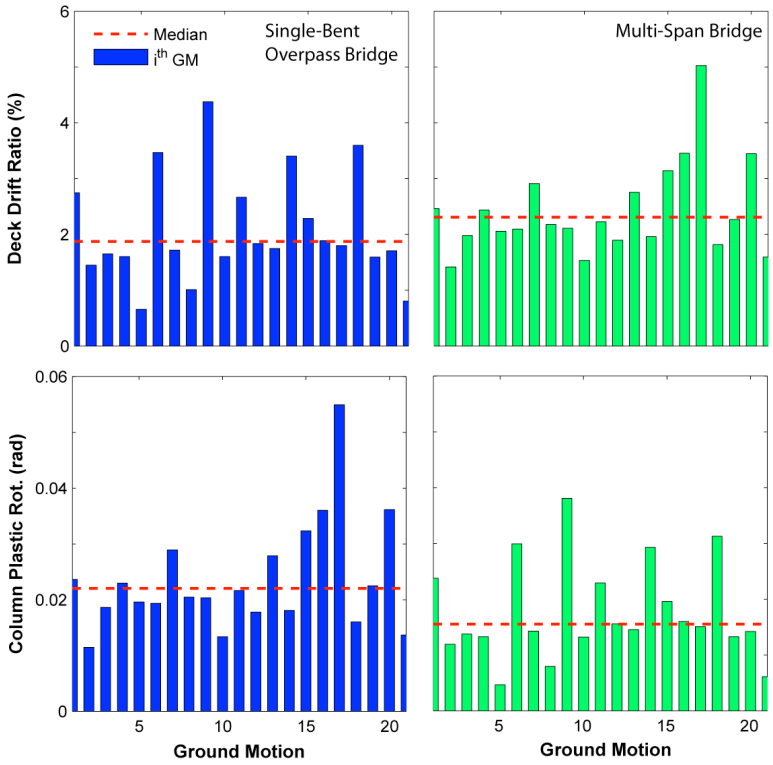

Figure 5. Median values of benchmark EDPs in transverse direction determined by nonlinear RHA of single-bent overpass [left panels] and multi-span bridge [right panels] due to 21 ground motions; results for individual ground motions are also included.

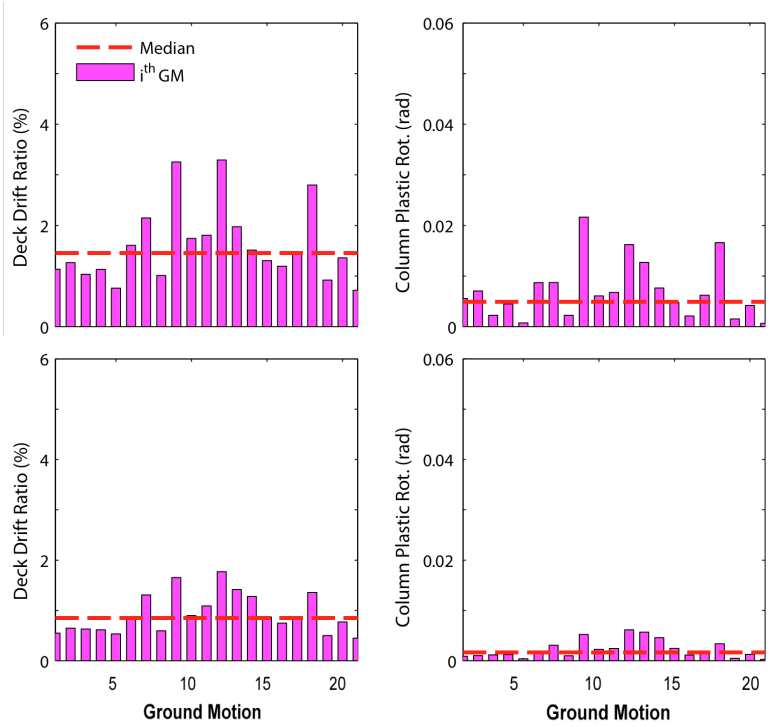

Figure 6. Median values of benchmark EDPs in transverse direction [top panels] and EDPs in longitudinal direction [bottom panels] determined by nonlinear RHA of curved bridge due to 21 ground motions; results for individual ground motions are also included.

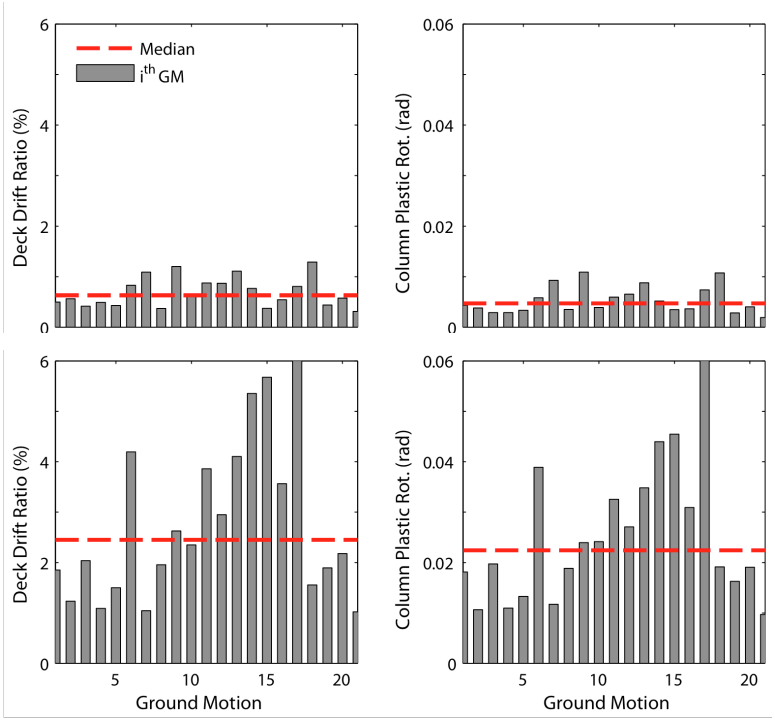

Figure 7. Median values of benchmark EDPs in transverse direction [top panels] and EDPs in longitudinal direction [bottom panels] determined by nonlinear RHA of skew bridge due to 21 ground motions; results for individual ground motions are also included.

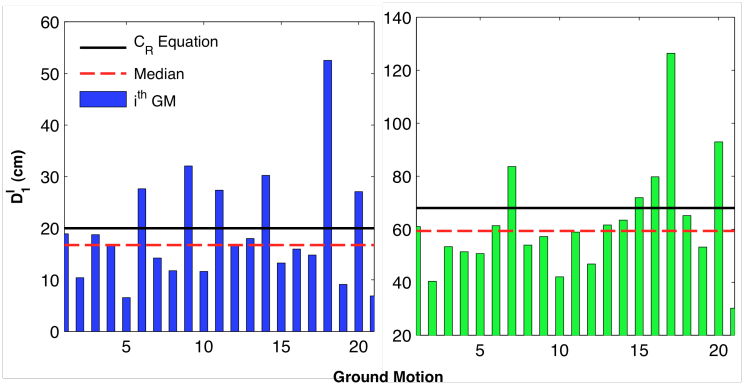

Figure 8. Peak deformation D_1^I values of the first-"mode" inelastic SDF system for 21 ground motions for single-bent overpass [left panel] and multi-span bridge [right panel]; "exact" target value of deformation $\bar{D}_1^I$ is identified by horizontal dashed line; horizontal continuous line indicates target value of deformation $\bar{D}_1^I$ established by the C_R equation.

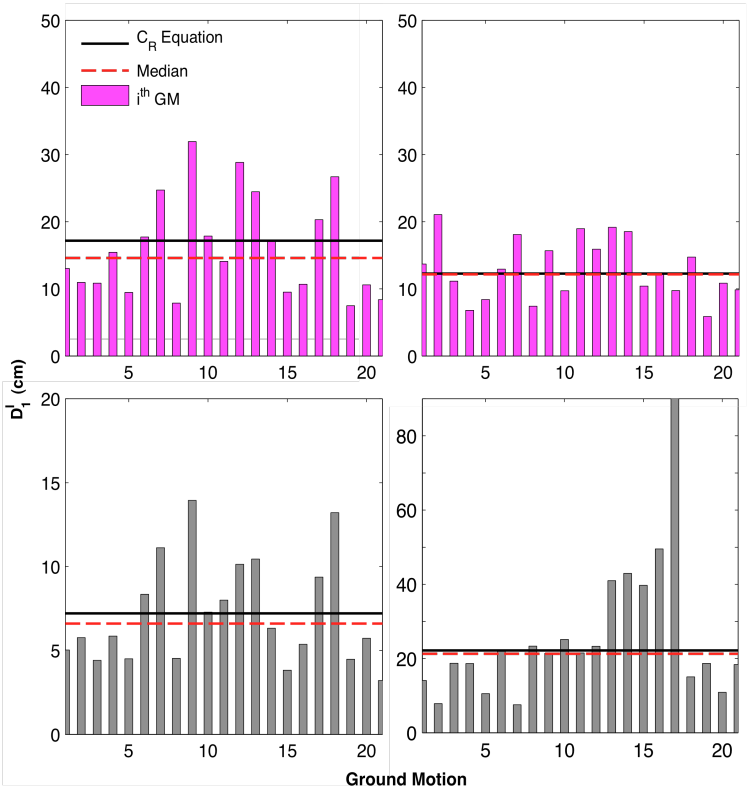

Figure 9. Peak deformation D_1^I values of the first-"mode" inelastic SDF system in the transverse direction [left] and in the longitudinal direction [right] for 21 ground motions for curved bridge [top panels] and skew bridge [bottom panels]; "exact" target value of deformation $\bar{D}_1^I$ is identified by horizontal dashed line; horizontal continuous line indicates target value of deformation $\bar{D}_1^I$ established by the C_R equation.

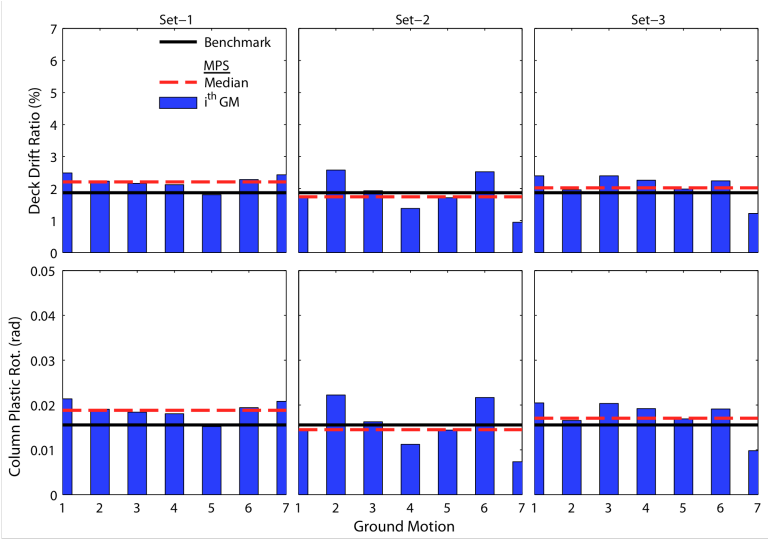

Figure 10. Comparison of median EDPs based on the MPS with benchmark EDPs for the single-bent overpass; individual results for each of the seven scaled ground motions are also presented.

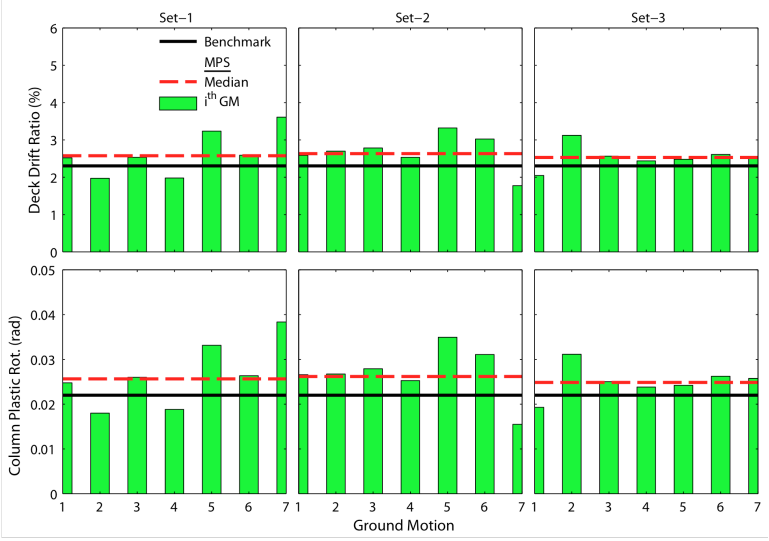

Figure 11. Comparison of median EDPs based on the MPS with benchmark EDPs for the multi-span bridge; individual results for each of the seven scaled ground motions are also presented.

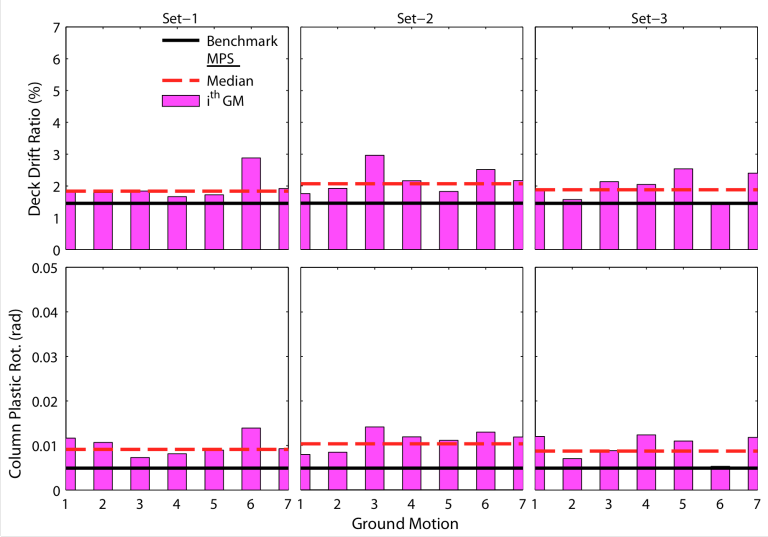

Figure 12. Comparison of median EDPs in transverse direction based on the MPS with benchmark EDPs for the curved bridge; individual results for each of the seven scaled ground motions are also presented.

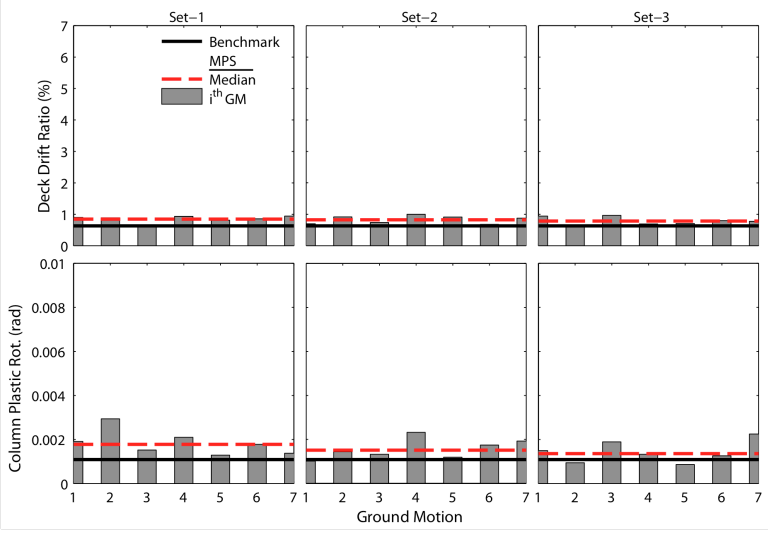

Figure 13. Comparison of median EDPs in transverse direction based on the MPS with benchmark EDPs for the skew bridge; individual results for each of the seven scaled ground motions are also presented.

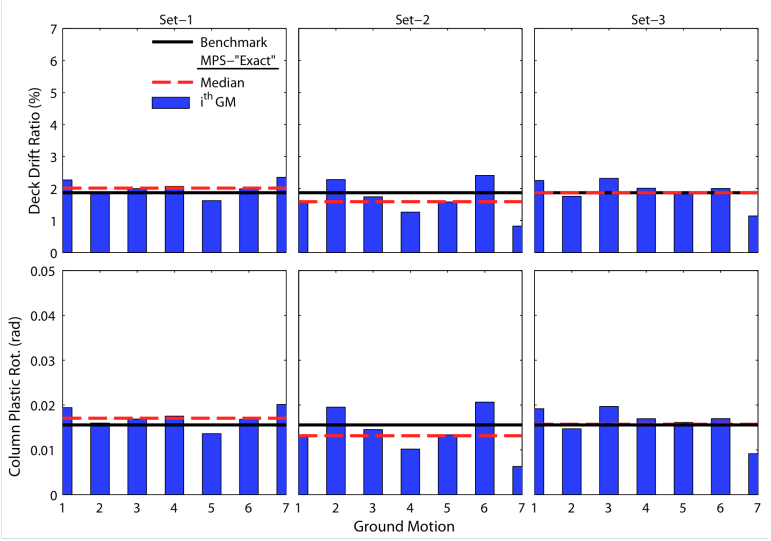

Figure 14. Comparison of median EDPs based on the MPS-“Exact” with benchmark for the single-bent overpass; individual results for each of the seven scaled ground motions are also presented.

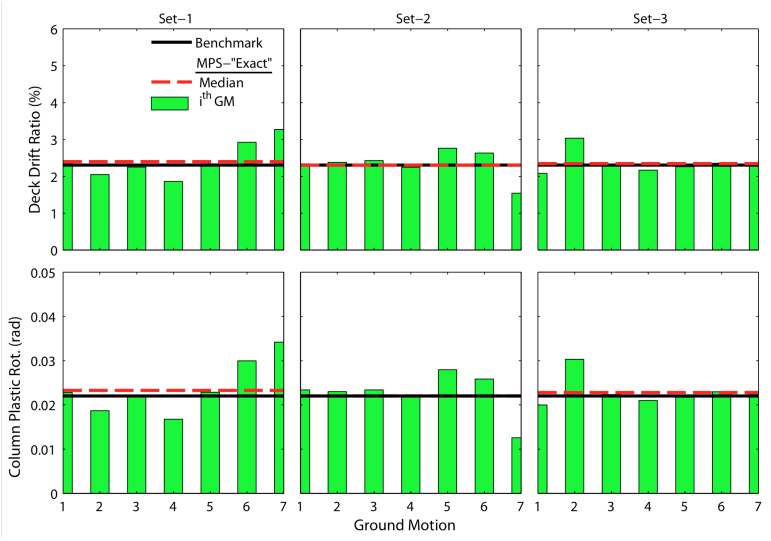

Figure 15. Comparison of median EDPs based on the MPS-“Exact” with benchmark EDPs for the multi-span bridge; individual results for each of the seven scaled ground motions are also presented.

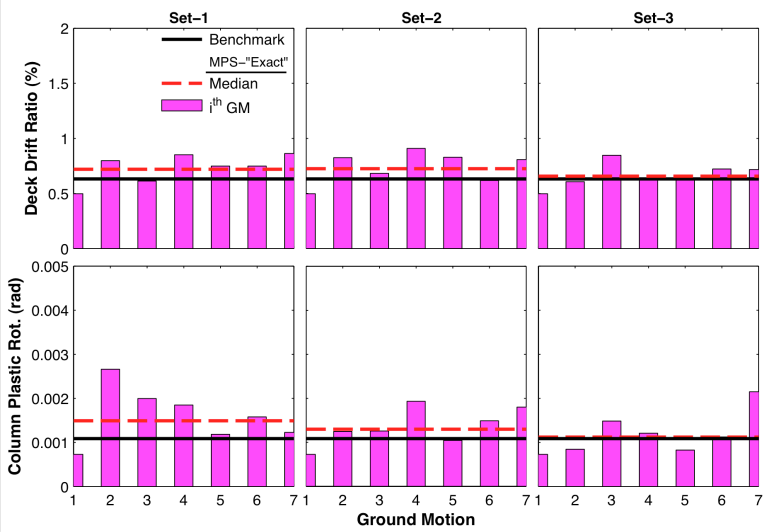

Figure 16. Comparison of median EDPs in transverse direction based on the MPS-"Exact" with benchmark EDPs for the curved bridge; individual results for each of the seven scaled ground motions are also presented.

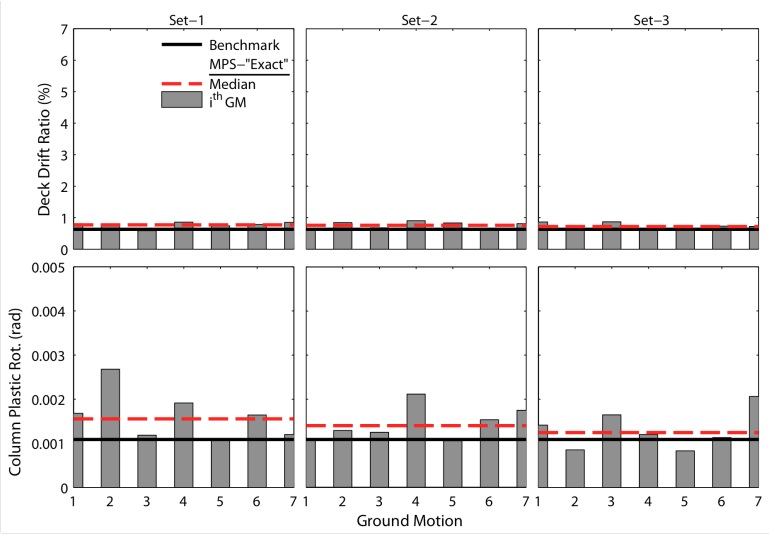

Figure 17. Comparison of median EDPs in transverse direction based on the MPS-"Exact" with benchmark EDPs for the skew bridge; individual results for each of the seven scaled ground motions are also presented.

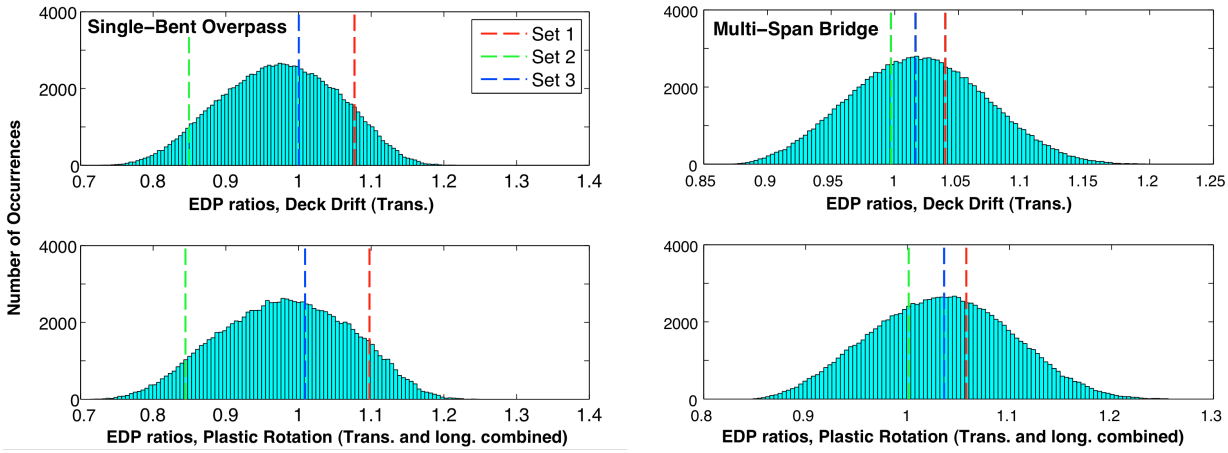

Figure 18. Distribution of median EDP ratios (EDP value ÷ benchmark value) based on the MPS-"Exact" for the single-bent overpass and multi-span bridge for more than 100,000 sets of seven ground motion records; median results from randomly selected three sets of seven records (Sets 1 through 3) are also shown using vertical dashed lines.